

(vii) the large-scale curvature of the cycloidal chains. Cracks that are not cycloidal must have propagated faster or originated from a different stress pattern, such as that due to nonsynchronous rotation (4, 6, 18).

If Europa's water layer were solid down to the silicate layer without a substantial liquid layer (tens of kilometers thick), then diurnal tidal stress would be inadequate to fracture the surface because the amplitude of the tidal variation would be too small. The creation of cycloidal cracks requires a global ocean to generate substantial tidal stress over a diurnal cycle. Even so, the formation of cycloidal cracks may require that the ice be weak, because the maximum tidal stress is <40 kPa (<0.4 bar).

With so little stress, how deep can the cracks penetrate? Geologic evidence of lateral motion, dilation, and strike-slip motion on Europa suggests that cracks (including cycloidal cracks) from the surface penetrate down to a low-viscosity layer (13-15, 19, 20), possibly an ocean. However, with less than 40 kPa of tensile stress, as in the case of our model of cycloidal cracks, the tensile stresses are overwhelmed by the compressive hydrostatic overburden pressure at the depth of only ~65m (21). These cracks could be driven to greater depths by the insertion of liquid water (22, 23) or of material due to mass wasting (analogous to a wedge) (6, 23). Cracks may also go to greater depth because additional stress is concentrated at the base of the crack (18), but even that concentration is unlikely to drive a crack from the surface much deeper than ~1 km.

However, Crawford and Stevenson (24) noted that a thicker crust could crack all the way through if the crack initiates at the bottom of the ice layer and liquid water mitigates the overburden pressure. They noted that initiating a crack at the bottom would be difficult because the ice at the base would be warmer and thus less brittle than the colder ice at the surface. They also pointed out that even if a crack could start, it could propagate upward through only nine-tenths of the thickness of the ice layer (that is, up to the float line), but they speculated that additional forces would be needed, perhaps from gases dissolved in the water, to drive the crack through the remainder of the ice up to the surface.

Even if such an ad hoc process acted, it is unlikely that cracks could penetrate more than a few kilometers on Europa. At that depth, they might reach a ductile ice layer, which in principle could have served as the low-viscosity layer for lateral motion (19, 25). However, the association of cracks with ridge pairs suggests that the cracks penetrate to liquid water and not just ductile ice (6, 10, 11, 20). Thus our model implies that Europa's ice crust overlies liquid water and is thin enough that cracks go all the way through.

Cycloidal lineaments on Europa appear to

have formed in response to diurnal tides, a process that occurs quickly over the course of a few days, at a rate of one cycloid per European day (3.551 Earth days). This theory provides a specific time scale that is remarkably short for a major type of geological feature. Other icy satellites do not appear to have any analog to European cycloids, which suggests that only Europa has the unique characteristics necessary to form cycloidal features: A global ocean, substantial diurnal tidal stress, and a weak lithosphere.

References and Notes

1. B. A. Smith et al., *Science* **206**, 927 (1979).
2. S. J. Peale, P. Cassen, R. T. Reynolds, *ibid.* **203**, 892 (1979).
3. P. Helfenstein and E. M. Parmentier *Icarus* **53**, 415 (1983).
4. ———, *ibid.* **61**, 175 (1985).
5. A. S. McEwen, *Nature* **321**, 49 (1986).
6. R. Greenberg et al., *Icarus* **135**, 64 (1998).
7. B. L. Lucchita and L. A. Soderblom, in *Satellites of Jupiter*, D. Morrison, Ed. (Univ. of Arizona Press, Tucson, AZ, 1982), pp. 521-555.
8. M. C. Malin and C. C. Pieri, in *Satellites*, J. A. Burns and M. S. Matthews, Eds. (Univ. of Arizona Press, Tucson, AZ, 1986), pp. 689-717.
9. J. W. Head et al., *J. Geophys. Res.*, in press.
10. S. D. Kadel et al., *Lunar Planet. Sci. Conf. XXIX* [CD ROM] (1998).

11. E. P. Turtle et al., *Eos* **79**, S202 (1998).
12. R. Sullivan et al., *Nature* **391**, 371 (1998).
13. B. R. Tufts et al., in preparation.
14. R. T. Pappalardo and R. Sullivan, *Icarus* **123**, 557 (1996).
15. M. Nolan and R. Greenberg, *Bull. Am. Astron. Soc.* **19**, 860 (1987).
16. G. V. Hoppa and B. R. Tufts, *Lunar Planet. Sci. Conf. XXX* [CD ROM] (1999).
17. P. H. Gammon, H. Klefte, M. J. Clouter, *J. Phys. Chem.* **87**, 4025 (1983).
18. A. C. Leith and W. B. McKinnon, *Icarus* **120**, 387 (1996).
19. P. M. Schenk and W. B. McKinnon, *ibid.* **79**, 75 (1989).
20. G. V. Hoppa et al., *Icarus*, in press.
21. R. A. Smith, *J. Glaciol.* **17**, 223 (1976).
22. G. W. Ojkangas and D. J. Stevenson, *Icarus* **81**, 242 (1989).
23. B. R. Tufts, thesis, University of Arizona, Tucson (1998).
24. G. D. Crawford and D. J. Stevenson, *Icarus* **73**, 66 (1988).
25. M. P. Golombek and W. B. Banderdt, *ibid.* **83**, 441 (1990).
26. We thank W. McKinnon for his careful review and suggestions for improving this work, especially his insight into the propagation process, and the members and affiliates of the Galileo SSI team, led by M. Belton, for their comments and suggestions. Theoretical aspects of this work were supported by grant 347050 from NASA's Planetary Geology and Geophysics program.

28 April 1999; accepted 4 August 1999

Ultrasonic Deposition of High-Selectivity Nanoporous Carbon Membranes

Mark B. Shiflett¹ and Henry C. Foley²

Ultrasonic deposition creates a thin film of polymer on a tubular, macroporous, stainless steel support. Using polyfurfuryl alcohol as the nanoporous carbon precursor and a pyrolysis temperature of 723 kelvin, a membrane was prepared with the following permeances, measured in moles per square meter per Pascal per second: nitrogen, 1.8×10^{-12} ; oxygen, 5.6×10^{-11} ; helium, 3.3×10^{-10} ; and hydrogen, 6.1×10^{-10} . The ideal separation factors as compared to that for nitrogen are 30:1, 178:1, and 331:1 for oxygen, helium, and hydrogen, respectively.

Molecular separations are energy-intensive processes that can be used in a wide spectrum of areas, ranging from emerging biotechnologies to more classical fuels and chemicals production. The global move toward greener production is necessarily coupled with the need for more energy-efficient, and hence novel, separations. Molecular separations based on differences in molecular size and shape using ceramic membranes (1, 2) at ambient temperature are particularly intriguing, because these materials can conduct such separations with less energy.

This approach is particularly important for the removal of water from biotechnological broths in which the hydraulic load is high, but it is just as much an issue for gas separations such as the separation of nitrogen (N₂) from air, which is done by energy-intensive cryogenic distillation. Ceramic, as opposed to polymeric, membranes can operate under harsh conditions and at elevated temperatures (3), such as occur in reactive separations. Zeolites (4), sol-gels (5), and nanoporous carbons (NPCs) (6) are each candidate materials for the preparation of novel size-selective ceramic membranes.

Continuous nanoporous carbon membranes can be prepared as thin films supported on porous stainless steel by means of ultrasonic deposition (UD) of polyfurfuryl alcohol (PFA). These supported nanoporous carbon mem-

¹DuPont Central Research and Development, Experimental Station, Wilmington, DE 19880, USA. ²Center for Catalytic Science and Technology, Department of Chemical Engineering, University of Delaware, Newark, DE 19716, USA.

REPORTS

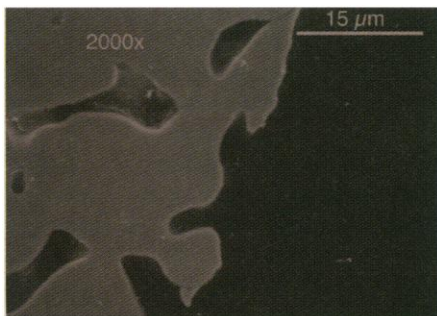


Fig. 1. An SEM radial image of the membrane surface.

branes (SNPCMs) show unprecedented size and shape selectivities, even among very small molecules with similar dimensions. Using the rate of N_2 permeation for comparison, hydrogen (H_2), helium (He), and oxygen (O_2) are transported through an SNPCM 330, 178, and 30 times faster. If the molecules were transported on the basis of Knudsen diffusion rather than on the basis of size selectivity, these transport ratios (H_2/N_2 , He/N_2 , and O_2/N_2) would be 3.73, 2.65, and 0.94, respectively. The ultrasonic deposition technique makes it possible to prepare membranes as films that are mechanically robust and selective but remain below a critical thickness for crack formation.

Membrane synthesis and fabrication have proven to be critical problems with these materials, because continuous films are difficult to achieve. Nanoporous carbon molecular sieves are disordered solids with densities between 70 and 80% of that of crystalline graphite. Nanopore dimensions range from 0.3 to 0.7 nm, with a maximum between 0.35 and 0.55 nm (7–10). These structural features, which are reminiscent of fullerene-like fragments, make the NPC molecular sieves ideally suited for the production of N_2 from air by kinetic separation (8, 9). Membranes consisting of NPC on support media offer a new and potentially more efficacious means to O_2/N_2 and other small-molecule separations (6).

Two types of NPC membranes have been prepared in the past: unsupported (planar monoliths and hollow fibers) and supported (asymmetric membranes) (11). The unsupported NPC materials provided high selectivities but suffered from extreme fragility. Recent work avoided this drawback by forming NPC layers on support media such as porous graphite and sintered stainless steel (6). These materials were more robust and displayed good selectivity but reproducibility was problematic. Polymer precursor deposition and pyrolysis are two of the key steps that must be precisely controlled to overcome this problem.

The membrane supports that we used were sintered stainless steel tubes (SS304, Mott Metallurgical) with an outside diameter of 6.35 mm, a wall thickness of 1.48 mm, and a nominal pore size of 0.2 μm , and were coated with

Table 1. Permeances and ideal separation factors for SNPCMs. The pyrolysis temperature for each sample is given. Thicknesses are calculated on the basis of final masses. Samples I through III were coated three times, and sample IV was coated six times.

Sample no.	Temperature (K)	NPC mass/thickness		Permeance						Separation factor		
		(mg)	(μm)	N_2	O_2	He	H_2	O_2/N_2	He/ N_2	H_2/N_2		
I	423	10.5	12.9	0	0	0	0	0	0	0		
II	573	18.6	22.9	0.786	10.6	125	138	13.5	160	175		
III	723	17.3	21.3	1.83	55.7	326	605	30.4	178	331		
IV	873	8.5	10.4	45.5	127	1080	1356	2.80	23.7	29.8		

PFA resin with an ultrasonic nozzle (12). The low-momentum deposition provided by an ultrasonic nozzle offers more precise control of the coating process as compared with conventional high-pressure gas spraying, including a 10^2 to 10^3 lower spray velocity that minimizes penetration into the support. The droplets are narrowly distributed in size from 10 to 100 μm , depending on nozzle operating frequency. The precursor delivery rate can be accurately controlled with a syringe pump. The coated tubes were then pyrolyzed (13), and upon completion of the heat treatment the furnace was shut off and the tubes were allowed to cool.

We prepared four membranes (SNPCM I through IV) whose total masses and NPC layer thicknesses are presented in Table 1. Typically, the first carbon layer ranged in mass from 8 to 11 mg, corresponding to a carbon yield of 20 to 30%, based on the wet coat mass. In successive steps after each heat treatment, we added less NPC per coat: Second coat masses were 5 to 7 mg, and third coat masses were 0.1 to 0.4 mg.

In the case of SNPCM-IV, however, three primary coatings with a total mass of 5 mg were put down, followed by three more coatings of 1.4, 1.0, and 1.1 mg.

Scanning electron microscope (SEM, Hitachi S-4000) images were taken of the exterior surface and of cross and axial sections of a sacrificial membrane. We prepared this membrane under the same conditions as those used for SNPCM-II. The micrograph (Fig. 1) reveals a film with a uniform radial thickness of $15 \pm 2 \mu\text{m}$. The axial profiles were similarly uniform, and the surface view showed a continuous defect-free coating.

In order to measure the gas permeance, the tubular membranes were inserted into a module that consisted of a cylindrical membrane holder with knife-edge flanges on either side sealed with copper gaskets. The flanged ends were welded to compression fittings. With external compression applied to the fittings, pressures up to 7000 kPa were maintained, with no measurable leakage at 295 K. Pressure-rise experiments were performed on all tubular membranes (14).

The N_2 permeance of another sacrificial membrane prepared in the same way as SNPCM-III was measured after the addition of each NPC layer. The N_2 permeance initially decreased as the NPC mass increased (Fig. 2A). Once a critical mass of NPC was reached, the last carbon layer added resulted in an increase in permeance and a concomitant loss in selectivity. An SEM analysis of this membrane film

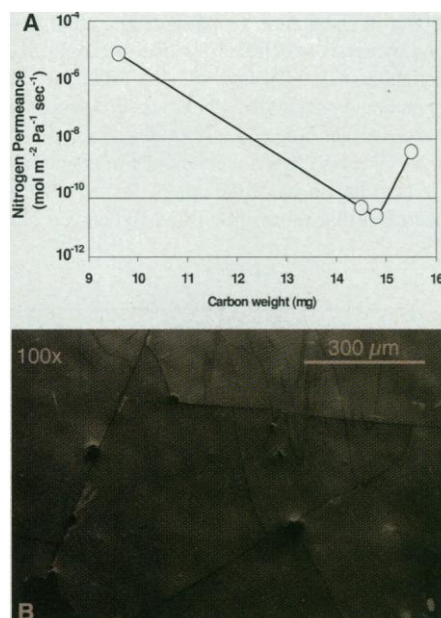


Fig. 2. (A) N_2 permeance as a function of carbon mass. (B) An SEM image of a cracked surface of a film 19.1 μm in thickness.

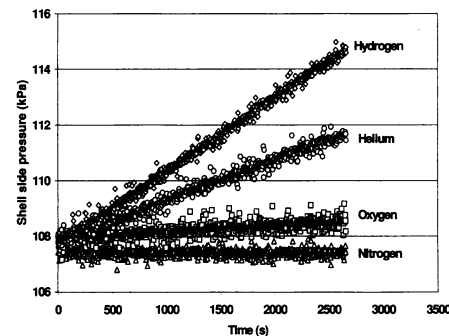
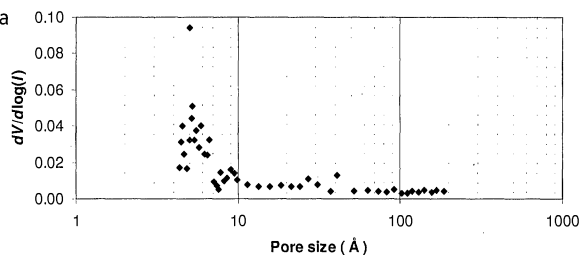


Fig. 3. Pressure rise as a function of time for sample SNPCM-III.

Fig. 4. Pore size distribution for a SNPCM.


revealed that catastrophic crack formation had occurred (Fig. 2B). In this case, the total mass of NPC on the support was 14.8 mg before the cracking process and 15.5 mg after. Given that the density of the NPC is 1.6 g/cm³ (9), these masses correspond to calculated thicknesses of 18.2 and 19.1 μm, respectively. Asymmetric films of this kind are known to have a critical thickness below which the film has mechanical properties that are more plasticlike than those of the bulk material (15). Based on these data, we can estimate that the onset of bulk-like NPC properties and catastrophic cracking occurs in the vicinity of a critical film thickness of 20 ± 3 μm. Thus, the deposition process must be carefully controlled in order to produce membranes below this thickness.

We sought to prepare the membranes (SNPCM-I through IV) so that the final masses of NPC produced films that were below the critical thickness. SNPCM-III consisted of three layers of NPC with corresponding masses of 11.0, 5.9, and 0.4 mg and calculated thicknesses of 13.5, 7.3, and 0.5 μm. The change in shell side pressure as a function of time for each gas shows that the slopes of the pressure-rise curves decrease with increasing molecular size (Fig. 3). There is a measurable difference between the slopes of these rates even for N₂ and O₂, which differ by only 0.02 nm in kinetic diameter (16). The small-molecule selectivity can be explained by examining the pore size distribution for a similar SNPCM prepared at 873 K with a mean pore size centered around an average of 0.50 μm. (Fig. 4). From the ideal gas law, the time rate of change in shell side pressure, P_{ss} , is (17)

$$\frac{dP_{ss}}{dt} = \frac{A \cdot R \cdot T}{V_{ss}} \cdot \frac{\pi'}{\delta} \cdot (P_{cs} - P_{ss}) \quad (1)$$

Integrating from the initial shell side pressure P_{ss0} at time $t_0 = 0$ to the final shell side pressure P_{ss} at $t_f = t$ results in

$$\frac{V_{ss}}{A \cdot R \cdot T} \cdot \ln \left| \frac{P_{cs} - P_{ss0}}{P_{cs} - P_{ss}} \right| = \frac{\pi'}{\delta} \cdot t \quad (2)$$

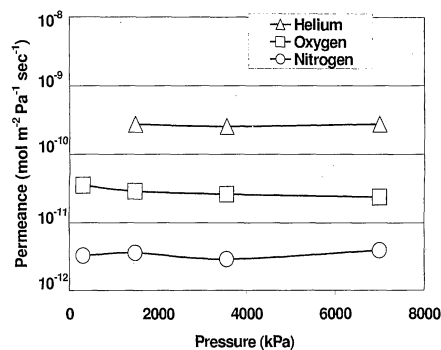
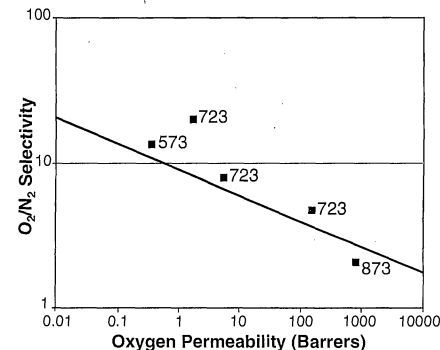
A plot of the left side of Eq. 2 versus time gives a straight line with a slope of

$$\frac{\pi'}{\delta} = \pi_0,$$

the gas permeance. Permeances and ideal separation factors (the ratio of permeance with respect to N₂ permeance) for SNPCM-III (Table 1) are 30 to 90 times greater than the calculated separation factors based on Knudsen diffusivities (16).

It was assumed in the integration of Eq. 1 that π_0 was independent of pressure. To test this assumption, the permeances were measured as a function of pressure from 300 to 7000 kPa and were found to be pressure-independent (Fig. 5). This result shows that there was no Poiseville flow through the membrane.

Finally, using UD to control thickness, the effect of membrane synthesis temperature during pyrolysis was tested by also preparing materials at 423, 573, and 873 K (Table 1). The membrane prepared at 423 K was impermeable, whereas that prepared at 873 K displayed permeabilities that were over an order of magnitude greater than those of the others. Its selectivities were less than those of SNPCM-III but were still


Fig. 5. Permeance as a function of pressure for sample SNPCM-III.

Fig. 6. O₂/N₂ selectivity versus O₂ permeability (π').

higher than the Knudsen values. These selectivities indicate that the membrane was not cracked but that the higher pyrolysis temperature brought on lower selectivity. When pyrolyzed at 573 K, the resulting membrane, SNPCM-II, showed good selectivities but not as high as those of the membrane prepared at 723 K. That thermal effects should play such a role in determining membrane properties, and hence selectivities, is expected on the basis of previous work with bulk NPC materials (9). O₂/N₂ selectivity versus O₂ permeability for SNPCM-II, -III, -IV, and two additional membranes prepared at 723 K are plotted versus the best known reported values (18), which lie on or below the dividing line (Fig. 6).

In addition to transient experiments, a steady-state experiment was run using SNPCM-III to separate air. High-pressure air from a gas cylinder was fed at a constant pressure of 3550 kPa to the core side of the membrane. The shell side operated at atmospheric pressure, and a gas chromatograph was used to analyze the permeate, which contained 44% oxygen, a 100% enrichment.

References and Notes

- J. N. Armor, *J. Membr. Sci.* **147**, 217 (1998); K. Keizer and H. Verweij, *Chemtech* **26**, 37 (1996).
- R. M. De Vos and H. Verweij, *Science* **279**, 1710 (1998).
- M. P. Harold and C. Lee, *Chem. Eng. Sci.* **52**, 1923 (1997); J. N. Armor, *Catal. Today* **25**, 199 (1995).
- Y. S. Yan, M. E. Davis, G. R. Gavalas, *J. Membr. Sci.* **123**, 95 (1997); L. C. Boudreau, J. A. Kuck, M. Tsatsis, *ibid.* **152**, 41 (1999); Y. G. Li, S. Yong, W. Z. Jiang, C. G. Peng, *Mater. Lett.* **37**, 221 (1998); H. H. Funke et al., *J. Membr. Sci.* **129**, 77 (1997); W. J. W. Bakker, F. Kapteijn, J. Poppe, J. A. Moulijn, *ibid.* **117**, 57 (1996).
- B. N. Nair, *J. Membr. Sci.* **135**, 237 (1997); H. Ohya, K. Masaoka, M. Aihara, Y. Negishi, *ibid.* **146**, 9 (1998).
- M. Acharya, B. A. Raich, H. C. Foley, M. P. Harold, J. J. Lerou, *Ind. Eng. Chem. Res.* **36**, 2924 (1997); Y. D. Chen and R. T. Yang, *ibid.* **33**, 3146 (1994); M. B. Rao and S. Sircar, *J. Membr. Sci.* **110**, 10 (1996); V. C. Geiszler and W. J. Koros, *Ind. Eng. Chem. Res.* **35**, 2999 (1996).
- H. C. Foley, *Micropor. Mater.* **4**, 407 (1995).
- J. N. Armor, *Adv. Chem. Ser.* **245**, 321 (1995); T. R. Gaffney, *Curr. Opin. Solid State Mater. Sci.* **1**, 69 (1996).
- M. S. Kane et al., *Chem. Mater.* **8**, 2159 (1996); M. Acharya et al., *Philos. Mag. B*, in press.
- R. K. Mariwala and H. C. Foley, *Ind. Eng. Chem. Res.* **33**, 2314 (1994); T. A. Braymer, *Carbon* **32**, 445 (1994); R. K. Mariwala and H. C. Foley, *Ind. Eng. Chem. Res.* **33**, 607 (1994).
- J. E. Koresch and A. Soffer, *Sep. Sci. Technol.* **22**, 973 (1987); J. E. Koresch and A. Soffer, *J. Chem. Soc. Faraday Trans. I* **82**, 2057 (1986).
- We cut the sintered tubes to a length of 25 mm and welded solid stainless steel tubing to both ends. The solid tubing was cleaned in an ultrasonic bath and dried in an oven for 2 hours at 393 K. After cleaning, we handled the tubes with Nitrile gloves and stored them in a dehumidified chamber. PFA resin was diluted with acetone to form a 25 weight % PFA solution. A syringe pump filled with this solution delivered the precursor to the ultrasonic nozzle at a rate of 1 cc/min. The ultrasonic nozzle, fabricated at DuPont, was powered by a Dukane ultrasonic generator and was operated at 40 kHz. With the ultrasonic nozzle held 6 mm above the surface, we rotated the porous metal tubes at 150 rpm and translated the nozzle in the axial direction at speeds ranging from 1 to 10 mm/s. Acetone evaporated from the wet coating while the tubes were rotated for an additional 10 min in air. The masses of the coatings were determined after this air-drying step. Depending on the axial coating

speed, 1 to 50 mg of PFA could be applied in each coating step.

13. The coated tubes were placed inside a quartz pipe 57 mm in diameter, fitted with end caps designed to hold the coated tubes in the center while they were being rotated. The quartz pipe was fitted into a temperature-controlled furnace and purged with scientific-grade He (total impurities <1 part per million) at a flow rate of 100 cc/min for 15 min. The temperature was raised at a rate of 5.0°C/min to the final temperature (473 to 873 K) and held there for 120 min. To ensure uniformity during pyrolysis, we rotated the tubes at 30 rpm.

14. The gas was introduced on the core (feed) side of the NPCM at a pressure of 300 kPa, and the shell side pressure response was measured continuously. The membrane module was evacuated and returned to atmospheric pressure on both the core and shell sides before the introduction of the next probe gas. All experiments were conducted at 295 K.

15. J. W. Hutchinson and Z. Suo, *Adv. Appl. Mech.* **29**, 63 (1991).

16. R. C. Reid, J. M. Prausnitz, B. E. Poling, *The Properties of Gases and Liquids* (McGraw-Hill, New York, ed. 4, 1987).

17. P_{ss} and P_{cs} (Pa) are the pressures on the shell side and core side of the tubular membrane, respectively; t (s) is time; A (m^2) is the membrane area; R ($m^3 Pa mol^{-1} K^{-1}$) is the gas constant; T (K) is the temperature; V_{ss} (m^3) is the shell side volume; π' is the gas permeability ($mol m^{-1} sec^{-1} Pa^{-1}$); and δ (m) is the membrane thickness.

18. L. M. Robeson, *J. Mem. Sci.* **62**, 165 (1991).

19. Supported by Department of Energy Office of Basic Energy Science, State of Delaware Research Partnership, and DuPont.

30 March 1999; accepted 9 August 1999

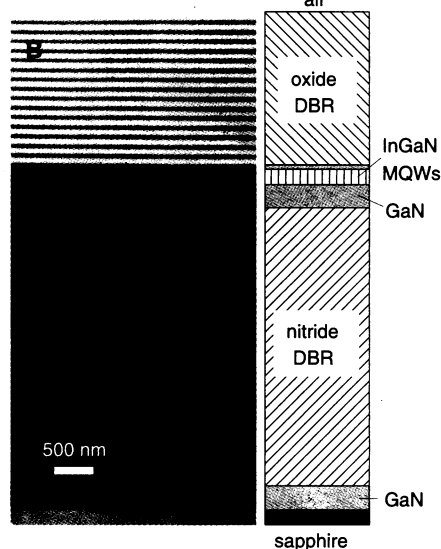
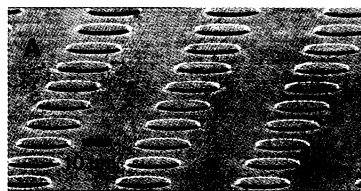
Room Temperature Lasing at Blue Wavelengths in Gallium Nitride Microcavities

Takao Someya,^{1*} Ralph Werner,² Alfred Forchel,² Massimo Catalano,³ Roberto Cingolani,⁴ Yasuhiko Arakawa¹

Lasing action has been demonstrated at blue wavelengths in vertical cavity surface-emitting lasers at room temperature. The microcavity was formed by sandwiching indium gallium nitride multiple quantum wells between nitride-based and oxide-based quarter-wave reflectors. Lasing action was observed at a wavelength of 399 nanometers under optical excitation and confirmed by a narrowing of the linewidth in the emission spectra from 0.8 nanometer below threshold to less than 0.1 nanometer (resolution limit) above threshold. The result suggests that practical blue vertical cavity surface-emitting lasers can be realized in gallium-nitride-based material systems.

Blue nitride-based semiconductor laser diodes (LDs) and light-emitting diodes (LEDs) have been developed over the past few years (1–13) and are having a large impact on industry as well as on fundamental research. Blue vertical cavity surface-emitting lasers (VCSELs) have attracted increasing attention (14, 15) because they are expected to surpass conventional blue nitride LDs in many applications. In particular, the use of two-dimensional arrays of blue VCSELs would drastically reduce the read-out time in high-density optical storage (compact disc and digital video disc) and increase the scan speed in high-resolution laser printing technology (14). The short vertical cavity configuration is also especially suitable for reducing the threshold current in blue lasers, because wide band gap materials have large optical gain due to the giant joint density of states (1, 2). In addition, field patterns from VCSELs are naturally completely circular, whereas the aspect

ratio between vertical and horizontal modes is still 4 in conventional edge-emitting nitride lasers (10).



The main obstacle to the room-temperature operation of blue VCSELs is the crystal growth of highly reflective nitride mirrors consisting of GaN and AlN or GaN and $Al_xGa_{1-x}N$ with high aluminum content x on which the high-quality InGaN active regions are subsequently grown (16–19). The problems that arise in epitaxial growth of high-quality films are the large difference in thermal expansion coefficients between GaN ($5.6 \times 10^{-6}/K$) and AlN ($4.2 \times 10^{-6}/K$) and the large difference in their lattice constants (2.7%) (20). However, progress in crystal growth technology is now opening the door to the synthesis of highly lattice-mismatched nitride semiconductor systems.

We report here the fabrication of blue nitride VCSELs and the observation of lasing action at room temperature. Using a microcavity with a high Q factor of 500, we observed lasing action at a wavelength of 399 nm under optical excitation.

Disk-shaped VCSEL structures 18 μm in diameter are formed from a planar multilayer by reactive ion etching and arrayed in a two-

Fig. 1. (A) Scanning electron microscope image of a two-dimensional array of GaN-based VCSELs. **(B)** Cross-sectional image of the VCSEL structure observed by transmission electron microscopy. The structure of the GaN-based multilayer, grown on a (0001)-oriented sapphire substrate, is as follows: a 30-nm GaN nucleation layer, 400-nm GaN, a nitride distributed Bragg reflector (DBR) consisting of 43 pairs of 38-nm GaN (dark layers) and 40-nm $Al_{0.34}Ga_{0.66}N$ (bright layers), 195-nm GaN, multiple quantum wells (MQWs) consisting of 26 periods of 5-nm $In_{0.01}Ga_{0.99}N$ barrier and 3-nm $In_{0.1}Ga_{0.9}N$ quantum well, and 18-nm GaN. The aluminum content $x = 0.34$ of the $Al_xGa_{1-x}N$ was determined by x-ray diffraction measurements. The oxide DBR consisting of 15 pairs of 48-nm ZrO_2 (dark layers) and 68-nm SiO_2 (bright layers) was evaporated on the top of the GaN-based multilayer to form a vertical cavity.

¹Institute of Industrial Science, University of Tokyo, 7-22-1 Roppongi, Minato-ku, Tokyo 106-8558, Japan.

²Lehrstuhl für Technische Physik, Universität Würzburg, Am Hubland, 97074 Würzburg, Germany. ³Consiglio Nazionale delle Ricerche, Istituto Studio Materiali per l'Elettronica, Università di Lecce, via Arnesano 73100 Lecce, Italy. ⁴Istituto Nazionale Fisica Materia, Università di Lecce, Dipartimento Ingegneria Innovazione, via Arnesano 73100 Lecce, Italy.

*To whom correspondence should be addressed. E-mail: someya@iis.u-tokyo.ac.jp